AD-A105 877 GEORGE WASHINGTON UNIV WASHINGTON D C DEPT OF CHEMISTRY F/G 7/4
INTERPRETATION OF THE NITROGEN KVV AUGER LINESHAPE FROM ALKALI --ETC(U)
OCT 81 F L HUTSON, D E RAMAKER, B I DUNLAP N00014-80-K-0852
UNCLASSIFIED TR-6 NL

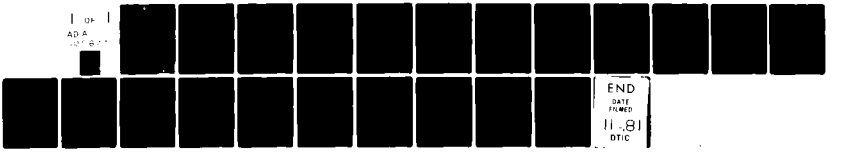

OFFICE OF NAVAL RESEARCH

N00014-80-K-0852

Task No. 056-681

Technical Report No. 6

Interpretation of the Nitrogen KVV Auger Lineshape from Alkali Metal Nitrates

by

P.L. Hutson, D.E. Ramaker, B.I. Dunlap, J.D. Ganjei, and J.S. Murday

Prepared for Publication

in the

Journal of Chemical Physics

George Washington University
Department of Chemistry
Washington, D.C. 20052

October 1981

SECURITY CLASSIFICATION OF THIS PAGE (When Data Entered)

REPORT DOCUMENTATION PAGE

READ INSTRUCTIONS BEFORE COMPLETING FORM

1. REPORT NUMBER: No. 6	2. GOVT ACCESSION NO.: AD A105877
3. RECIPIENT'S CATALOG NUMBER:	
4. TITLE (and Subtitle): Interpretation of the Nitrogen KVV Auger Lineshape from Alkali Metal Nitrates	5. TYPE OF REPORT & PERIOD COVERED: Technical Report
6. PERFORMING ORG. REPORT NUMBER:	
7. AUTHOR(s): F.L. Hutson, D.E. Ramaker, B.I. Dunlap, J.D. Ganjei, and J.S. Murday	8. CONTRACT OR GRANT NUMBER(s): N00014-80-K-0852
9. PERFORMING ORGANIZATION NAME AND ADDRESS: Chemistry Department, George Washingotn University, Washington, D.C. 20052	10. PROGRAM ELEMENT, PROJECT, TASK AREA & WORK UNIT NUMBERS: Prog. Elem. No. 61153N; Task Area No. PP 013-08-01; Work Unit No NR 056-681
11. CONTROLLING OFFICE NAME AND ADDRESS: Office of Naval Research, Dept. of Navy, 800 N. Quincy Street, Washington, D.C. 22217	12. REPORT DATE: Oct 1981
	13. NUMBER OF PAGES: 40
14. MONITORING AGENCY NAME & ADDRESS(if different from Controlling Office)	15. SECURITY CLASS. (of this report): Unclassified
	15a. DECLASSIFICATION/DOWNGRADING SCHEDULE:

16. DISTRIBUTION STATEMENT (of this Report)

This document has been approved for public release and sale; its distribution is unlimited.

17. DISTRIBUTION STATEMENT (of the abstract entered in Block 20, if different from Report)

18. SUPPLEMENTARY NOTES

Submitted for publication in the Journal of Chemical Physics

19. KEY WORDS (Continue on reverse side if necessary and identify by block number)

Auger electron spectroscopy, nitrates, oxyanions, molecular orbital populations

20. ABSTRACT (Continue on reverse side if necessary and identify by block number)

Experimental N KVV Auger lineshapes from sodium nitrate, produced by both x-ray (XEA) and electron (EEA) excitation, are compared to theoretically derived lineshapes based on populations derived from a GTO-LCAO-Xα model. The one-electron orbital energies and valence line widths are determined from x-ray emission and photoelectron data; the Auger matrix elements are determined from experimental gas phase atomic Auger data. The theoretical Auger energies include hole-hole repulsion and relaxation. Theoretical lineshapes

DD FORM 1 JAN 73 1473 EDITION OF 1 NOV 65 IS OBSOLETE S/N 0102-014-6601 | Unclassified SECURITY CLASSIFICATION OF THIS PAGE (When Data Entered)

using the local and the Mulliken X_α populations are generated, and a set of empirical populations are also determined. This work emphasizes the importance of shake-off arising from creation of the initial core hole and its effect on the Auger lineshape. A theoretical shake/Auger satellite lineshape is generated and found to contribute up to 35% of the total intensity. The XEA and EEA lineshapes (after correction for the sample and spectrometer transmission response) each show five features, but some differences are noted. These are attributed primarily to beam damage and charging effects on the EEA lineshape. The theoretical lineshapes reproduce the five principal features of the experimental spectra; specific features in the lineshape are shown to reflect the relative size of the Auger matrix elements, the symmetry of the NO_3^- ion, and satellite contributions. Arguments for the validity of a one-electron orbital model to describe the Auger lineshape are presented.

INTERPRETATION OF THE NITROGEN KVV AUGER LINESHAPE FROM ALKALI METAL NITRATES

F.L. Hutson*, D.E. Ramaker*, and B.I. Dunlap*

Department of Chemistry
George Washington University
Washington, DC 20052

and

J.D. Ganjei and J.S. Murday

Naval Research Laboratory
Washington, DC 20375

* Supported in part by the Office of Naval Research.

ABSTRACT

Experimental N KVV Auger lineshapes from sodium nitrate, produced by both x-ray (XEA) and electron (EEA) excitation, are compared to theoretically derived lineshapes based on populations derived from a GTO-LCAO-Xα model. The one-electron orbital energies and valence line widths are determined from x-ray emission and photoelectron data; the Auger matrix elements are determined from experimental gas phase atomic Auger data. The theoretical Auger energies include hole-hole repulsion and relaxation. Theoretical lineshapes using the local and the Mulliken Xα populations are generated, and a set of empirical populations are also determined. This work emphasizes the importance of shake-off arising from creation of the initial core hole and its effect on the Auger lineshape. A theoretical shake/Auger satellite lineshape is generated and found to contribute up to 35% of the total intensity. The XEA and EEA lineshapes (after correction for the sample and spectrometer transmission response) each show five features, but some differences are noted. These are attributed primarily to beam damage and charging effects on the EEA lineshape. The theoretical lineshapes reproduce the five principal features of the experimental spectra; specific features in the lineshape are shown to reflect the relative size of the Auger matrix elements, the symmetry of the NO_3^- ion, and satellite contributions. Arguments for the validity of a one-electron orbital model to describe the Auger lineshape are presented.

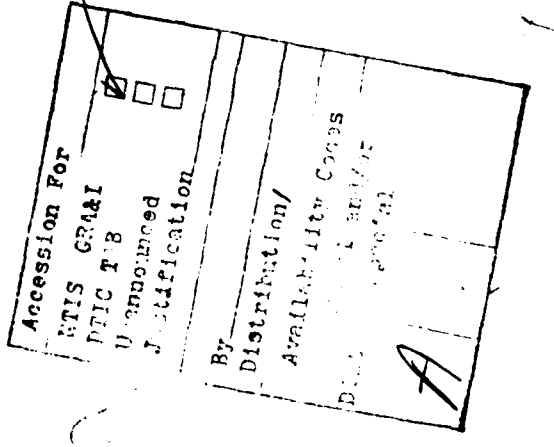

I. Introduction

From a theoretical viewpoint, the Auger process is a complicated dynamical process exhibiting several interesting phenomena. These include: i) possible localization of the Auger final state holes as a result of electron correlation, ii) a "Coulomb explosion" of the local cluster as a result of the final localized holes, and iii) atomic relaxation and electron screening as a result of the initial core hole. We report here results of an interpretation of the N KVV lineshape from an alkali metal nitrate (1). The contrast of a highly covalent oxyanion in a highly ionic lattice allows us to clarify these Auger phenomena more easily.

Recently we reported results of an interpretation of the X(X = Si, P, or S) $L_{23}VV$ Auger lineshapes of the third row species SiO_2, PO_4^{3-}, and SO_4^{2-} (2-6). The theoretical treatment here is similar, however, this work includes for the first time, a determination of a shake Auger satellite lineshape. Although in our previous work (4,6) we attributed contributions arising between the main Auger features to shake-Auger satellites, we did not attempt to generate a theoretical shake Auger lineshape. The more complete description allows for a more critical comparison with experiment in this work. The NO_3^- oxyanion has several characteristics different from the third row oxyanions; thus it provides a good additional test of the Auger theory.

Three aspects of the electron density of states (DOS) will be examined with regard to the Auger lineshape. First, the N KVV Auger process involves a 1s initial core hole, the $L_{23}VV$ process studied earlier involved a 2p initial hole. The associated Auger transition matrix elements caused the $L_{23}VV$ Auger spectra to be dominated by the *pp contributions* (*i.e., the most probable transitions* leave both of the final state holes in the 3p atomic orbitals) (4). In the N KVV case, the pp contributions still are the largest; however, the ss contributions relative to the pp are increased by a factor of ~ 4 (4). Second, the XO_4^{n-} oxyanions reflected a final DOS appropriate for a tetrahedral T_d structure, the NO_3^- ion is trigonal planar, D_{3h}. The lower symmetry reduces the orbital degeneracy of the final DOS and increases the resolved structure in the lineshape. Finally, the radial extent of the DOS sampled by the Auger, X-ray emission, and photoemission processes are of interest. We have performed GTO-LCAO-Xα calculations on the NO_3^- anion, determined the Mulliken and local charge populations, and compared them with previous theoretical calculations and with the experimental data.

The X $L_{23}VV$ Auger signal from the third row oxyanions, located around 100 eV, was difficult to separate from the large secondary contribution in this region (7). Reasonable signal to background ratios were obtained by recording the derivative of the Auger signal (dN/dE) to discriminate against the secondary contribution. This requires a rather high intensity electron excitation beam. The higher energy ($\sim$ 375 eV) of the N KVV signal is sufficiently removed from the secondaries to be conveniently recorded in the pulse count mode with either an x-ray or a low intensity electron excitation beam. The availability of these two different excitation sources in principle allows a test of the generality of the background removal procedure (7); however, charging and beam damage effects limits the accuracy of this test.

II. Experimental

A. Procedure

The Auger data was taken in three different experimental modes: using an x-ray excitation beam (XEA) with pulse count detection, using an electron beam (EEA) with pulse count detection, and using an electron beam with lock-in derivative detection. In Table 1 we summarize the experimental parameters used.

All analyses were performed using a Physical Electronics combined XPS/AES spectrometer, utilizing the double pass CMA Model 15-255G. The XPS and XEA measurements were made with a Mg x-ray anode source. EEA measurements were performed with the CMA coaxial electron gun. Signal averaging was accomplished with a Nicolet Model 1074 multichannel analyzer synchronized with the CMA.

Two-types of samples were utilized. A $NaNO_3$ sample was prepared by pressing the powdered sample into In foil. Complete coverage avoided the In MNN Auger transition at 408 eV which would interfere with the N KVV Auger signal. A $NaNO_3$ single crystal, cleaved immediately before introduction into the sample chamber, was also utilized. The Mg X-ray source was used so that the Na 1s photoelectron peak, which falls at 414 eV with an Al source, did not interfere with the N KVV Auger lineshape.

It has been shown that the NO_3^- ion decomposes to NO_2^- under exposure to an electron beam and that X-ray photoelectron spectroscopy (XPS) serves as an effective monitor of the beam damage (8). In this work each sample was analyzed by XPS both before and after the Auger data was taken. The XPS data revealed little damage except for the sample analyzed by the electron beam lock-in derivative mode where damage was of the order 5-20%. This was due to the higher intensity of the electron beam required in the derivative mode.

B. Data Reduction

Figure 1 shows the data as obtained from the three experimental collection modes. The N(E) data was convoluted with a 3.3 eV wide (11 points) sliding least-squares smoothing function due to Savitzky and Golay (9). This smoothing function nicely removes the noise with wavelength from 1 to 4 eV without significantly distorting the Auger lineshape with peak widths $\geq$ 10 eV. The dN/dE data is sufficiently smoothed by the integration process as shown in Figure 1. The actual or 'true' Auger lineshape $A_T(E)$ must be extracted from the N(E) signal by solving the equation,

$$N(E) = E^{\ell}B(E) + \int T(E,E')\, A_T(E')\, dE', \qquad (1)$$

where B(E) is the background and $T(E,E')$ is the instrument and sample response function. The procedure for accomplishing this has been reported previously (7). The energy loss and instrument response function $T(E,E')$ is approximated by the backscattered spectrum of an electron beam with primary energy equal to the energy of the principal Auger peak. B(E) must be scaled by E (ℓ = 1 in Eq. (1)) in the normal mode and by E^{-1} (ℓ = -1 in Eq. (1)) in the retard mode to account

for the change in the analyzer transmission over the breadth of the Auger signal (9); this scale factor must also be incorporated in $T(E,E')$ (see Eq. 20, Ref. 7).

The background is assumed to have the form

$$B(E) = \frac{AE}{(E+E_o)(E+\phi)^m} + \frac{B \ln[(E_p-E)/E_b]}{[(E_p-E)/E_b]^n} + C \qquad (2)$$

where A, B, and C are determined by a linear least squares fit to the background on each side of the Auger spectrum. The first term in Eq. (2) accounts for the true secondary electrons which decrease in intensity with increasing energy in the N KVV Auger region, the second term accounts for the redistributed primary electrons which increased in intensity with increasing energy in the same region. Estimates of E_o, ϕ, and E_b can be determined from theoretical considerations (7). E_p is the primary beam energy. In this work m and n were set to 2 and 1 respectively based on our previous results.

The generality of Eq. (2) can be tested by the differences between XEA and EEA data. In the EEA data, E_p is determined by the 2000 eV primary beam. E_b is determined by least squares to be = 950 eV (i.e., an effective average between the nearest loss features arising from the excitation of the O 1s and Na 1s electrons with binding energies of 532 and 1075 eV respectively). In this instance the redistributed primary electrons dominate the background so that smaller background contributions such as the O and Na KVV Auger electrons are removed along with the redistributed primaries. In the XEA data no primary electrons exist. However, the O KVV Auger electrons at $\approx$ 512 eV still appear just above the N KVV signal; some of these electrons suffer loss and appear in the N signal as background. These are removed in this instance by Eq. (2) with $E_p \approx$ 512 eV and $E_b \sim$ 13 eV (i.e. loss from valence electron excitation). Loss contributions from the O_{1s} and N_{1s} photoelectron peaks also appear in the background, but their energy dependence is small enough in this region to subtract them via the constant C. Fig. 1 illustrates the different background characters for the three data collection modes. Despite these differences in background character, Eq. (2) is

able to approximate the background with just three linear least squares parameters and a non-linear least squares value for E_b.

III. Theory

A. Characterization of Auger Transitions

The electronic structure of the NO_3^- ion is described here in terms of the linear combination of atomic orbitals-molecular orbital (LCAO-MO) model. The Auger transitions involve the N 1s core hole coupling with the valence molecular orbitals. Each KVV′ transition is represented by a Gaussian function characterized by an energy $E_{KVV'}$, an intensity $I_{KVV'}$, and a linewidth $\Gamma_{KVV'}$. Details of our empirical approach have been reported previously (2); they are briefly summarized here. A thorough examination of various ab-initio approaches to the interpretation of Auger lineshapes of small molecules has been given recently by Agren (11); however, the basic expressions for $E_{KVV'}$ and $I_{KVV'}$ are the same as those given below.

The transition energies are determined by the expression

$$E_{KVV'} = E_K - E_V - E_{V'} - U_{VV'} \tag{3a}$$

$$U_{VV'} = \sum_{nm} c_{Vn}^2 c_{V'm}^2 (f(n,m) - r_n \delta_{nm}) \tag{3b}$$

where the $E_K(E_V)$ are one electron M.O. binding energies as determined from XPS data. $U_{VV'}$ is a final state hole-hole interaction energy, which includes a static relaxation term due to the relaxation of the electrons in the presence of the two holes. c_{Vn}^2 are the populations of the atomic orbitals ϕ_n in the V^{th} molecular orbital, f(n,n) are atomic Coulomb repulsion integrals, and r_n(≈ 6 eV) is an intra-atomic orbital static relaxation energy (12). The one-center f(n,m) integrals are obtained from Mann's tables (13), the two center integrals from an appropriate interpolation scheme (3).

The intensities are calculated from the expression

$$I_{KVV'} = \sum_{ab} c_{Va}^2 c_{V'b}^2 P_{cab} \tag{4}$$

where c_{Va}^2 and $c_{V'b}^2$ are the populations of the atomic orbitals ϕ_a and ϕ_b located on the N atom in the V,V′ M.O.'s and P_{cab} is the appropriate atomic Auger matrix element

$$P_{cab} = \sum_{\ell} |\langle \phi_c k\ell | r_{12}^{-1} | \phi_a \phi_b \rangle|^2, \tag{5}$$

where ϕ_c and kℓ are the core and continuum orbitals respectively. The matrix elements are determined empirically from Ne gas data where the Auger transitions are sufficiently resolved to enable a determination of the individual intensities (i.e. ss, sp, pp, etc.). The Ne intensities may be used for N because of the small dependence on atomic number of these intensities for low Z (4). Eq. 4 reduces to a single term for the N atom in NO_3^-. It has been called the "one center intensity model" (11) and assumes that the Auger process probes electron populations only on the core hole site.

The linewidths are approximated by the expression

$$\Gamma_{KVV'} = \Gamma_K + \Gamma_V + \Gamma_{V'} + 2K \tag{6}$$

where $\Gamma_K(\Gamma_V)$ are the core (valence) level widths as determined from XPS and XES data and 2K is the singlet-triplet splitting. When 2K is larger than the other contributions to the width, the singlet and triplet final state transitions are considered separately with energies $E_{KVV} \pm K$.

B. M.O. Energies, Populations, and Widths

A number of M.O. calculations for NO_3^- have been reported in the last ten years (14-16). Most useful for our purposes are those of Dolin et al (16) which report the M.O. atomic populations. In this work we also use results of a GTO-LCAO-Xα calculation (17). The 5s/3p optimized GTO basis set as given by van Duijneveldt (14) for the N and O free atoms was supplemented with a diffuse s and p orbital

to accommodate the negative charge which exists on both the N and O atoms in NO_3^-. The basis set is essentially of single zeta quality (18) consistent with our need to identify unambiguously the N and O 2s and 2p "free atom like" populations. This need arises from our use of empirical P_{cab} values in Eq. (4). Complete theoretical evaluation of the Auger matrix elements involving the full M.O.'s does not require this identification; however, such a numerical evaluation is difficult and use of the empirical P_{cab} includes intra-atomic correlation which can be very significant (see Sec. III. D).

The M.O.'s in Table 2 are labeled according to the representations of the D_{3h} symmetry for a planar trigonal molecule. It is convenient also to label the M.O.'s according to their principal components. Thus, the $3a_1'$, $2e'$, and $4a_1'$ M.O.'s are referred to as the O_{2s} orbitals or the $N_{s'}$, $N_{p'}$, and N_s orbitals respectively; the $1a_2''$, $3e'$, and $4e'$ as the N_p or O_{2p} bonding orbitals; and the $1a_2'$ and $1e''$ as the O_{2p} nonbonding orbitals. The M.O. energies reported in Table 2 are obtained from XPS data (20). The widths are estimates obtained from XES and XPS data (19,20).

We report in Table 2 two different M.O. populations for the Xα calculation, the Mulliken and local. They are defined by the M.O. overlap equation

$$\sum_{nm} c_n c_m S_{nm} = \sum_n (c_n^2 + \sum_{m \neq n} c_n c_m S_{nm}) = 1. \tag{7}$$

The Mulliken populations include the "bonding" charge such that

$$P_n^M = c_n^2 + \tfrac{1}{2} \sum_{m \neq n} c_n c_m S_{nm} \tag{8}$$

and satisfy the sum rule

$$\sum_n P_n^M = 1. \tag{9}$$

The local populations include only the diagonal terms $P_n^L = c_n^2$.

It is generally accepted that the Auger process samples populations only on the atom with the core hole, but the extent of the radial wave function sampled by the Auger process is not clear. In some sense the local and Mulliken populations reflect different radial extent as the Mulliken population includes the bonding charge between the atoms, the local population excludes this charge. In an analysis of the $L_{23}VV$ Auger lineshape of elemental Si, it was reported that the local populations (with substantially decreased "s" populations on Si relative to the Mulliken) are more appropriate for predicting the Auger lineshape (21). However, in an analysis of the Si $L_{23}VV$ Auger lineshape in Pd_4Si and at the Pd/Si interface (22, 23), a self-fold of the Mulliken populations gave excellent agreement with experiment. This difference has been attributed to a contraction of the s orbitals on Si in Pd_4Si relative to elemental Si.

A simple analysis of the Auger matrix element states the Mulliken-local population question clearly but does not provide a simple answer. Consider a two atom system with $\Psi_V = a\phi_a + b\phi_b$ normalized such that $a^2+b^2+2abS = 1$ ($S=\langle\phi_a|\phi_b\rangle$). The CVV Auger intensity arising from a core hole on atom a is

$$\begin{aligned} I_{CVV} &\propto [\langle\phi_c k\ell|\frac{1}{r_{12}}|\Psi_V \Psi_V\rangle]^2 \\ &= [\langle\phi_c k\ell|\frac{1}{r_{12}}|a^2\phi_a^2 + b^2\phi_b^2 + ab\phi_a\phi_b + ba\phi_b\phi_a\rangle]^2 \\ &= [a^2 M_{caa} + b^2 M_{cbb} + abM_{cab} + baM_{cba}]^2 \end{aligned} \tag{10}$$

where the atomic Auger matrix elements are defined $M_{cab} = \langle\phi k\ell|\frac{1}{r_{12}}|\phi_a\phi_b\rangle$, etc. Now performing the square and keeping only the dominant terms we obtain the expression,

$$I \propto a^4 M_{caa}^2 + a^2 ab(M_{cab} + M_{cba})M_{caa} + \cdots, \tag{11}$$

where we assume that $M_{cbb} \ll M_{cab}, M_{cba} \ll M_{caa}$ (i.e., interatomic matrix elements are much smaller than intra-atomic elements).

The use of the local populations,

$$I \propto (P_{aa}^L)^2 M_{caa}^2 = a^4 M_{caa}^2, \tag{12}$$

is valid provided all interatomic matrix elements are indeed negligible. In this instance the local populations are also more appropriate for the x-ray emission and valence photo emission processes. This arises because of the highly localized

nature of the core N_{1s} orbital (not relevant for the valence PES process) and the nature of the continuum orbital for the high energy Auger or photoelectron (not relevant for the XES process). The PES process preferentially samples the electron density local to each nucleus, the XES and AES processes that local to the nucleus with the core hole.

The use of Mulliken populations gives the result,

$$I \alpha (P^M_{aa})^2 M_{caa}{}^2 = (a^2 + abS)^2 M_{caa}{}^2 = a^4 M_{caa}{}^2 + 2a^2 abS M_{caa}{}^2 + \ldots \qquad (13)$$

The second terms in Eqs. (11) and (13) are equivalent if

$$(M_{cab} + M_{cba})/M_{caa} = 2S$$

A semi-empirical analysis by Matthews and Komminos (24) indicates that the ratio $(M_{cab} + M_{cba})/M_{caa} \sim 10^{-2}$. Typical two center overlaps are of the order 10^{-1}.

The above analysis suggests that the local populations underestimate the Auger intensity at the bottom of the valence band (when the second term of Eqs. (11) and (13) is positive and the Mulliken populations overestimate this intensity. The complete reverse is true at the top of the band. However, one expects that at the bottom (top) of the band, the atomic orbital ϕ_a would be radially contracted (extended) compared to the free atomic orbital thus increasing (decreasing) P_{caa} compared with the free atom empirical value. This would move the correct result in the direction of the Mulliken and away from the local population estimate. It is not clear, however, which estimate would be closer to the experimental value.

Mulliken populations offer a distinct empirical advantage since they satisfy the sum rule, Eq. (9). Using XES and XPS data and Eq. (9), we were able to determine empirical populations which were satisfactory for interpreting the Auger lineshapes in the systems SiO_2, PO_4^{3-} and SO_4^{2-} (1-6). In this work we test the Xα Mulliken and local populations with XES, XPS, and AES data and also determine an empirical set of populations which are forced to satisfy the sum rule. Since the populations used in Eqs. (3a,b) and (16) to determine U must satisfy the

sum rule, we use either the theoretical Mulliken or the empirical populations to determine the Auger energies.

C. Auger Satellites

Auger satellites are clearly resolved in gas phase Auger spectra and may constitute up to 40% of the spectral intensity (25, 26). These satellites arise when Auger decay occurs in the presence of a spectator hole which shifts the Auger kinetic energy down from the parent peak. The spectator hole is created by the shake-off process, arising during the ionization of the core electron which initiates the Auger process (27).

Hole creation by the shake-off process is normally treated theoretically by the sudden approximation which is accurate for high impact energy. The magnitude of the energy available for shake-off $E-E_i$ (E is the beam energy, E_i the ionization energy) over the shakeoff energy E_o has been proposed as a good indicator of the degree to which the high energy limit has been reached (24). Experimental data reveals that the sudden approximation is valid when $(E-E_i)/E_o \gtrsim 3$ for photons, $(E-E_i)/E_o \gtrsim 10$ for electrons (28). For ionization of the N atom by a 1400 eV photon or a 2000 eV electron, these parameters are in the 60 to 100 range. The sudden approximation should be valid in this work.

The probability for shakeoff P_V in the sudden approximation and within the LCAO-MO theory can be approximated by (4)

$$P_V = 1 - \{1 - c_a^2 + c_a^2 (1-P_a)^{1/2n}\}^{2m}, \qquad (14)$$

where P_a is the atomic shake-off probability for N, c_a is the N atomic orbital contribution in the V^{th} M.O. and m(n) is the number of electrons in the M.O. (atomic shell). P_a is estimated (4) to be .12 and .42 for the N 2s and 2p filled shells, respectively. The resultant Auger satellite intensity $I_{KV-VV'V''}$ is related to the parent Auger intensity $I_{KV'V''}$ (4,27) by

$$I_{KV-VV'V''} = ((N-i)/N) \frac{P_V}{1-P_V} I_{KV'V''}, \qquad (15)$$

where i = 1 if V = V′ or V″, i = 2 if V = V′ = V″ and i = 0 otherwise.

The shift in energy of the satellite from the parent Auger peak has been treated by Shirley (29) for atoms. It has a similar form in the M.O. picture for molecules,

$$\Delta E_{KV\text{-}VV'V''} = U_{KV} - U_{VV'} - U_{VV''} , \qquad (16)$$

where the interaction energies U have been defined previously. A basic assumption in the Shirley model is that the energy of the three hole final state resulting from the shake/Auger process can be determined from a sum of two hole interaction energies (i.e., it assumes pairwise additivity).

The widths of the shake satellite peaks are assumed to be equal to the parent Auger widths. This is of course a rough approximation but adequate for our purposes because of the large number of shake satellites which tend to spread the satellite intensity over much of the Auger spectral region in any case. One might anticipate that the actual satellite widths may be a little larger than the parent Auger width because of the increased multiplet splitting in the final three-hole state of the satellite.

D. Electron Correlation

The Xα theory includes some aspects of local electron correlation; however, it is a one-electron model and cannot include all the dynamic correlation effects. The full consequences of electron correlation are most interesting. The most important is the tendency toward localization of the final state holes. A detailed treatment of electron correlation and localization in covalent systems has been reported by Ramaker ([3]). Application to the NO_3^- system is reported elsewhere (6). The essential result is that the 2 or 3 final state holes delocalize evenly about the entire NO_3^- anion, however, they cannot get off the anion. Thus, the NO_3^- one-electron M.O.'s give the best approximation to the final state hole-hole interaction energy $U_{VV'}$. Included in $U_{VV'}$ is a static relaxation term which arises from the relaxation of the electrons in the presence of the two holes (i.e., electron correlation within the cluster).

We assume in both Eqs. (3a,b) and (16), that the NO_3^- geometry (i.e., the N-O bond length) remains fixed even in the presence of 2 or 3 holes. Since doubly or triply ionized molecules are usually unstable (30), the resultant NO_3^+ (or NO_3^{2+}) anions likely suffer a "Coulomb explosion" breaking up the anion. The "Coulomb explosion" has been proposed as a mechanism for the observed beam damage and supported by semi-quantitative agreement with experimental damage cross sections (31). However, within the usual Born-Oppenheimer approximation, we assume that the Auger or shake/Auger electron is far removed from the anion before significant breakup of the anion occurs. Thus some broadening of the Auger lineshape may occur, but the effective U obtained from the NO_3^- M.O.'s is still appropriate.

In the initial state, electron correlation contributes to atomic relaxation, electron screening, and core hole-valence hole localization. The shake process is a direct result of the atomic relaxation and electron screening which occurs in response to the core hole. We distinguish here between relaxation of the valence atomic orbitals and actual transfer of electron density from a neighboring atom to the atom with the core hole (i.e., electron screening). It has been demonstrated that the former leads primarily to shake-off while the latter leads to shake-up (32,33). Shake-off leads to Auger satellites shifted down in energy by an amount ΔE given by Eq. (16), shake-up leads to satellites with generally smaller shifts either up or down in energy. Thus, we ignore the effects of electron screening in Eq. (14). The probability for shake P_V is determined from the unscreened electron M.O. populations; it includes only the shake-off contribution arising from the atomic relaxation. The core hole-valence hole localization mechanism holds the valence hole on the anion suffering the Auger event. If the valence hole could get sufficiently distant from the core hole before the Auger event, ΔE would become negligible and the Auger satellites would be eliminated.

The Auger intensities as expressed by Eqs. (4) and (5) also depend on electron correlation; indeed for the one-electron model to be rigorously valid, the initial and final state M.O.'s ought to be the same. As a simple approximation one can choose between two alternatives; either the initial or final state M.O.'s be used in Eq. (4). Our use of P_{cab} determined from gas phase data improves this approximation; the effects of atomic relaxation between the initial and final states are included in these empirically derived values. The effects of electron screening enter in the M.O. populations in Eq. (4). Use of the initial state populations increases the Auger intensity relative to use of the final state; however, only non-uniform changes across the lineshape are evident since only relative intensities are examined here. Von Barth and Grossman (34, 35) and others (36, 37) have found that at least for x-ray emission and absorption, use of the final state (a core hole is present for absorption, no core hole for emission) within a one-body theory gave satisfactory agreement with both the more complete dynamical theory and with experiment; use of the initial state leads to poor agreement. Having shown that a similar situation exists for the Auger process (38), and assuming that electron screening of the final valence holes is negligible, we evaluate the theoretical ground state populations by direct comparison to XPS, XES, and AES data. The best argument for this assumption is the agreement with experiment obtained in our earlier work on SiO_2, SO_4^{2-} and PO_4^{3-}. We test these ideas further in this work.

IV. Discussion

A. Comparison of experimental lineshapes

In Figure 2 we compare the electron excited Auger (EEA) lineshape in both the pulse count and normal derivative modes with the x-ray excited (XEA) lineshape. These lineshapes are obtained after removal of the background and deconvolution of the loss and analyzer response as summarized in Sec. IIB. The modulation broadening which occurs in the derivative mode has also been deconvoluted from the derivative mode EEA lineshape.

The pulse count and normal derivative mode EEA lineshapes have been shifted down in energy by amounts 1.4 eV and 1.7 eV respectively to bring the principal peaks of each EEA lineshape into registry with the XEA lineshape. These shifts can be attributed to sample charging. The required negative shifts suggest that either the electron excited sample is negatively charged and/or the x-ray excited sample is positively charged, both logical possibilities. The greater shift required for the normal derivative mode data reflects the larger electron beam intensity (1000 times greater than for the pulse count mode) with its increased effects of surface charging.

The three lineshapes are in qualitative agreement, however significant differences do appear. First we consider differences between the derivative and pulse count EEA lineshapes. The two lineshapes were obtained from different samples (see Table I); however, we don't believe this is the major source of the significantly broadened features of the derivative mode data. More significant is the larger current intensity for the derivative mode with its increased effects of surface charging and beam damage. A nonuniform surface charge density can significantly broaden the Auger features (39). XPS analysis before and after the Auger data acquisition revealed greater beam damage (see Table I) in the derivative case. As indicated earlier, the NO_3^- ion is converted to NO_2^- under electron irradiation (8). This has the effect of introducing a shoulder around 380 eV apparent in all 3 lineshapes. The Auger lineshape from a NO_2^- sample has increased intensity in the 370 to 385 eV range compared to the 320 to 360 range (1). The apparent greater damage in the derivative case may account for the decreased intensity in the 320 to 360 eV range; however, background subtraction and deconvolution may also lead to differences in this region.

If the resolution of the spectral features is taken as a measure of the quality of the lineshapes, the quality ranks in the order XEA > EEA-PC > EEA-LID. The intensity of the 'damage' shoulder at 380 eV also suggest the XEA lineshape was taken with the least damage, an observation consistent with the XPS observed data. Nevertheless, the shoulder at 381 eV does suggest some damage even in this case. For

Mg x-rays, the N 1s photoelectron is less surface sensitive than the lower energy Auger electron, therefore the XPS data does not detect the damage as quickly as the Auger.

B. Comparison of theory with experiment

Figure 3 compares the XEA lineshapes with the total theoretical lineshape (Auger plus the Auger/shake lineshape) generated from the local and Mulliken populations as described in Section III. The total theoretical lineshapes have been shifted by -2 to -3 eV to bring the principal peak into registry with the experimental peak; some of this can be attributed to a 4 to 5 eV spectrometer work function term which has not been included in the theoretical energies, Eq. (3a,b). The agreement to within 2 eV in absolute energy between theory and experiment using U=9 eV suggests that the two final state holes are indeed localized on a single NO_3^- anion. (Assuming complete delocalization would give U=0, localization on the N atom would give U=12 eV; localization on the NO_3^- anion gives U=9 eV (5)). The absolute intensity of the theoretical lineshape has been scaled to match the experimental lineshapes at the principal peak.

Comparison of the Xα local and Mulliken populations and those of Dolan and Dyatkina (DD) with the experimental XES and XPS data are given in Table 3. The XPS intensities are determined primarily by N_{2s} and O_{2s} electrons (except for the highest peak), the O K_α intensity by O_{2p} electrons, and the N K_α intensity by N_{2p} electrons. We have labeled each major contribution by its appropriate source (e.g. N_p etc.). As suggested in Sec. III. B, comparison of the O K_α and XPS data indicate the local populations underestimate (overestimate) the intensity at the bottom (top) of the band; the Mulliken populations overestimate (underestimate) this intensity. Examination of Table 3 and comparison of the Auger lineshapes in Fig. 3 do not indicate a clear preference overall between the Mulliken and local populations. The local populations appear to predict more closely the N K_α and Auger data, the Mulliken more closely the O K_α and XPS data; however, this may be fortuitous as the relative differences are within the accuracy of the Xα basis set.

The increased Np'/Np ratio for the Xα Mulliken populations is clearly in disagreement with the N K_α data. The calculations of Dolin and Dyatkina also clearly overestimate this ratio. Note that the N K_α XES experimental ratio of Np'/Np~11/89 is too small to give good agreement with the Auger lineshape (compare the experimental and empirical N K_α intensities). This disparity might be attributed to an error in the experimental XES estimate of the very small Np' intensity, as slight background corrections in this very broad peak would significantly alter its intensity (19). The empirical N K_α intensities do fall between the Xα local and Mulliken N K_α intensities as expected.

Table 4 presents an empirical set of populations chosen to best reproduce all of the data. These populations are made to satisfy the sum rule, Eq. (9) so that they can also be used to evaluate U, Eqs. (3a,b) and (16). Where the experimental data and the sum rule did not sufficiently define the population, the theoretical Xα and Dolan-Dyatkina populations were used as a guide. Comparison with the XES and XPS data is given in Table 3, comparison with the N KVV Auger lineshape is given in Fig. 4a. Except for the N XES Np'/Np ratio, excellent agreement is maintained, consistent with our earlier work in SiO_2.

Fig. 4b shows the Auger and shake satellite contributions to the total theoretical lineshape. Figure 4c compares the theoretical shake-off lineshape with the difference between the total experimental lineshape and the theoretically calculated Auger lineshape. Features are present with comparable intensity and energy in the two estimates of shake-off. The theoretical intensity is low at the higher energies around 375 to 390 eV reflecting possible contributions from NO_2^- resulting from beam damage. The shake intensity is approximately 35% of the total and reflects the same general features as the Auger lineshape, but with different intensities and shifted down in energy. The relative satellite shift $\Delta E^{\sim} \sim -6$ eV is predicted by Eq. (16) to within an eV utilizing the NO_3^- M.O.'s. (An adjustment in ΔE of $\sim$ 1 eV improved the total overall agreement between theory and experiment).

This indicates the 3 holes are delocalized about the NO_3^- anion as discussed previously (6).

Figure 4d and 4e compare the relative size and shape of the ss, sp, and pp contributions to the Auger and shake-Auger lineshapes. The source of each feature in the ss, sp, pp curves is indicated in Table 5. The pp contributions are clearly the largest, however, significant ss and sp contributions are also present. Indeed the entire low energy feature at 332 eV and most of the 355 eV feature result from the ss and sp contributions. The increased relative size (compared with the 3rd row oxyanions) of the quantity (ss + sp)/(pp) reflects matrix element effects due to the 1s initial core hole of the NO_3^- ion. The pp contribution alone exhibits 4 features (Fig. 4d), the two on the high energy side (at 373 and 380 eV) arising from the splitting of the N 2p orbitals into the $4e'$ and ($3e'$, $1a_2''$) M.O.'s reflecting the low D_{3h} symmetry of the NO_3^- ion. This splitting is large enough to cause the high energy shoulder at 380 eV. The peak at 355, the feature not present in the pp contributions, arises from s'p contributions. Thus, as we initially suggested, both the symmetry and the Auger matrix elements are reflected in the final total Auger lineshape.

The Auger lineshape provides a measure of the N 2s/2p population ratio. The ($s's'$, $s'p'$) and ($s's$, $s'p$) contributions at 335 and 355 eV respectively are underestimated by both the Xα local and Mulliken populations. Since the $N_s/N_{s'}$ ratio agrees reasonably well with the XPS data, this suggests strongly that the N_{2s} population in both the $3a_1'$ and $4a_1'$ M.O.'s are too small. The N_{2s} populations of Dolin and Dyatkina lend support to this point. If the N_{2s} population in the $4a_1'$ orbital were increased, the ss and sp contributions at 371 and 373 eV respectively, would not appreciably alter the lineshape in this region. This discussion of course assumes that the background subtraction and deconvolution procedure (which can give errors in the low energy end of the spectrum), and the $N\ P_{css}/P_{cpp}$ and P_{csp}/P_{cpp} matrix element ratios are correct.

Why did the Xα calculation underestimate the apparent N_{2s} population? Two possibilities can be suggested. First, core hole screening in sp metals appears to occur primarily via the s electrons (40, 41). However, the highly covalent nature of the NO_3^- system makes this less likely. The Dolin and Dyatkina calculation predicts a proper N_{2s} density without involving core hole screening, and the final state, which was suggested in Sec. III. D as more appropriate for describing the lineshape, has no core hole. The other possibility involves the basis set used in the Xα calculation. The O_{2s} total Mulliken charge of 2.23 electrons/atom appears unreasonably large. This may indicate that our limited Gaussian basis set is inadequate and the calculation artifically places too much s electron density on the O atoms. Use of an extended Gaussian basis set might improve the s/p population balance, but would be difficult to reconcile with our use of empirical atomic matrix elements.

V. Conclusion

In summary, the NO_3^- electron excited and photon excited Auger lineshapes reveal some differences; beam damage and charging in the electron excited case can account for these differences. All features (their intensities and energies) of the experimental XEA lineshape are predicted by the theory. Comparison with experimental data does not indicate a clear preference for the use of the Xα local or Mulliken populations. The Auger lineshape is seen to reflect the molecular symmetry and the relative size of the Auger matrix elements. The importance of the Auger/shake satellites are emphasized; the energy shift of the satellites are predicted satisfactorily.

References

1. *F.L. Hutson*, "The Analysis of the N KVV Auger Lineshape for the NO_3^- Anion," Masters Thesis submitted to George Washington Univ. (unpublished).
2. D.E. Ramaker, J.S. Murday, N.H. Turner, C. Moore, M.G. Lagally, and J. Houston, Phys. Rev. B19, 5375 (1979).
3. D.E. Ramaker, Phys. Rev. B21, 4608 (1980).
4. D.E. Ramaker and J.S. Murday, J. Vac. Sci. Technol. 16, 510 (1979).
5. J.S. Murday, D.E. Ramaker, M.K. Bernett, and N.H. Turner, Proc. Int. Vac. Congr. 7th 2, 1293 (1977).
6. B.I. Dunlap, F.L. Hutson, and D.E. Ramaker, J. Vac. Sci. Technol. 18, 556 (1981).
7. *D.E. Ramaker, J.S. Murday, and N.H. Turner, J. Electron Spect. Related* Phen. 17, 45 (1979).
8. T. Sasaki, R.S. Williams, J.S. Wong, and D.A. Shirley, J. Chem. Phys. 68, 2718 (1978).
9. A. Savitzky and M.J.E. Golay, Anal. Chem. 36, 1627 (1964); see also H.H. Madden and D. G. Schreiner, Sandia Laboratories Research Report SAND76-0283, 1976 (unpublished).
10. R.W. Springer and D.J. Pocker, Rev. Sci. Instrum. 48, 74 (1977).
11. H. Agren, J. Chem. Phys. 75, 1267 (1981).
12. *D.A. Shirley, Phys. Rev.* A7, 1520 (1973); Chem. Phys. Lett. 16, 220 (1972); 17, 312 (1972).
13. J.B. Mann, Los Alamos Scientific Laboratory Report LASL-3690, 1967 (unpublished).
14. M. Barber, J.A. Connor, I.H. Hillier, and V.R. Saunders, "Electron Spectroscopy", D.A. Shirley, ed., (North Holland, Amsterdam, 1972), p. 379; J.F. Wyatt, I.H Hillier, V.R. Saunders, J.A. Connor, and M. Barber, J. Chem. Phys. 54, 5311 (1971).
15. W.H. Morrison, Jr., and D.N. Hendrickson, Inorg. Chem. 11, 2600 (1972).
16. S.P. Dolin and M.E. Dyatkina, J. Struct. Chem. 13, 906 (1972).
17. B.I. Dunlap, J.W.D. Connolly, and J.R. Sabin, J. Chem. Phys. 71, 3396 (1979); 71, 4995 (1979).
18. F.B. van Duijneveldt, IBM Research Report RJ 945 (1971).
19. N. Kosuch, E. Tegeler, G. Weich, and A. Faessler, J. Electron Spect. Related Phen. 13, 263 (1978).
20. A. Calabrese and R.G. Hayes, J. Electron Spect. Related Phen. 6, 1 (1975).
21. D.R. Jennison, Phys. Rev. Letters 40, 807 (1978).
22. S.D. Bader, L. Richter, and M.B. Brodsky, W. E. Brower and G. V. Smith, *Solid State Communications* 37, 729 (1981).
23. G.W. *Rubloff*, P.S. Ho, J.F. Freeouf, and J.E. Lewis, Phys. Rev. B23, 4183 (1981).
24. J.A.D. Matthew and Y. *Komninos, Surf. Sci.* 53, 716 (1975).
25. H. Korber and W. Mehlhorn, Z. Physik 191, 217 (1966); W. Mehlhorn, D. Stalherm, and H. Verbeek, Z. Naturforsch 23A, 287 (1968).
26. M.O. Krause, T.A. Carlson, and W.E. Moddeman, J. Phys. Coll. C4 32, 139 (1971); M.O. Krause, F.A. Stevie, L.J. Lewis, T.A. Carlson, and W.E. Moddeman, Phys. Lett. 31A, 81 (1970).
27. E.J. McGuire, Phys. Rev. A11, 1880 (1975).
28. T.A. Carlson, Radiation Research 64, 53 (1975).
29. D.A. Shirley, Phys. Rev. A9, 1549 (1974).
30. T.A. Carlson and M.O. Krause, J. Chem. Phys. 56, 3206 (1972).
31. D.E. Ramaker, C.T. White, J.S. Murday, J. Vac. Sci. Technol. 18, 748 (1981).
32. W. Domcke, L.S. Cederbaum, J. Schirmer, and W. von Niessen, Phys. Rev. Letters 42, 1237 (1979).
33. W. Domcke, L.S. Cederbaum, J. Schirmer, and W. von Niessen, Chemical Physics 39, 149 (1979).
34. U. von Barth and G. Grossmann, Solid State Communications 32, 645 (1979).
35. U. von Barth and G. Grossmann, Physica Scripta 21, 580 (1980).
36. G.D. Mahan, Phys. Rev. B21, 1421 (1980).

37. V.I. Grebennikov, Y.A. Babanov, and O.B. Sokolov, Phys. Stat. Sol. 80, 73 (1977).

38. D.E. Ramaker, submitted to Phys. Rev. B.

39. T.E. Gallon and J.D. Nuttall, Surf. Sci. 53, 698 (1975).

40. D.R. Jennison, H.H. Madden, D.M. Zehner, Phys. Rev. B21, 430 (1980).

41. R. Lasser and J.C. Fuggle, Phys. Rev. B22, 2637 (1980).

Table 1. Summary of Experimental Parameters

Parameter	XPS	XEA	EEA (Pulse count)	EEA (Derivative)
Excitation source	Mg anode	Mg anode	2000 eV e^- beam	2000 eV e^- beam
Beam intensity			10^{-8} Amp/cm^2	10^{-5} Amps/cm^2
CMA mode	Retard, PE 50	Retard, PE 100	Retard, PE 100	Normal 5V$_{p-p}$ mod.
Damage Observed	Negligible	Negligible	Very slight	5-20% est.
Sample		$NaNO_3$ pressed powder	$NaNO_3$ pressed powder	$NaNO_3$ single crystal

Table 2. M.O. Energies, Linewidths and Populations for the NO_3^- Ion

Orbital[a]	Binding Energy (eV)[b]	Width (eV)[c]	Dolin & Dyatkina[d]				X_α Local Populations[e]				X_α Mulliken Populations[e]			
			N_{2s}	N_{2p}	O_{2s}	O_{2p}	N_{2s}	N_{2p}	O_{2s}	O_{2p}	N_{2s}	N_{2p}	O_{2s}	O_{2p}
$1a_2''$	5.6					.67				.75				.67
$1e''$						1.33				1.51				1.33
$4e'$	7.5	1.5		.55	.02	1.13		.46	.36	1.37		.37		1.21
$3e'$	11.9	1.7		1.50	.41	.42		.96	.99	.41		.76	.53	.55
$1a_2'$	13.3	3		.60		.47		1.00		.15		1.26		.25
$4a_1'$	14.5	2	.72		.37	.05	.59		.51	.11	.51		.38	.18
$2e'$	26.2	4		1.00	.93	.07		.50	.91	.12		.89	.89	.14
$3a_1'$	31.7	3	.85		.29	.09	.44		.32	.04	.31		.43	.13
Total			1.57	3.69	2.02	4.23	1.03	2.92	3.10	4.46	.62	3.28	2.23	4.46
N_{1s}	407.5	.2												
Charge N/O			-.26		-.25						+1.09		-.69	

[a]Orbitals labeled according to D_{3h} symmetry.
[b]XPS binding energies given by Kosuch et. al. (19).
[c]Widths as estimated from XPS and XES data (19,20).
[d]Electrons per atom as reported by Dolin and Dyatkina (16).
[e]Electrons per atom (local and Mulliken) as determined by our X_α calculations.

Table 3. Comparison of M.O. Populations with Experimental Data

	Orbital Type	X_α Local	X_α Mulliken	DD[a]	Exp[b]	Emp[c]
Nitrogen K_α						
N_p	$4e'$, $3e'$, $1a_2''$	15	11	15	8	14
N_p'	$2e'$	67	62	58	81	69
		17	27	27	11	17
Oxygen K_α						
O_{2p}	$4e'$, $1e''$, $1a_2'$	82	72	74	74	71
	$3e'$, $1a_2''$	13	18	20	14	18
O_{2s}	$4a_1'$	2	4	1	4	3
	$2e'$	2	3	2	5	3
	$3a_1'$	1	3	2	1	4
XPS[a]						
	$O_{2p(nb)}$ $1e''$, $1a_2'$	18	11	11	12	12
N_p	$O_{2p(b)}$ $4e'$, $3e'$	26	20	16	14	15
$N_{p\pi}$	$1a_2''$	18	19	22	21	21
N_s	$4a_1'$					
N_p	O_{2s} $2e'$	37	32	32	39	36
N_s'	$3a_1'$	11	18	18	12	15

[a]XPS matrix elements from Calabrese and Hayes (20) (i.e., N_{2s} = 8.8, N_{2p} = .8, O_{2s} = 10.3, O_{2p} = 1.0).
[b]N and O K_α data from Kosuch (19), XPS data from Calabrese and Hayes (20).
[c]Empirical populations as described in text.

Table 2. M.O. Energies, Linewidths and Populations for the NO_3^- Ion

Orbital[a]	Binding[b] Energy (eV)	Width[c] (eV)	Dolin & Dyatkina[d]				X_α Local Populations[e]				X_α Mulliken Populations[e]			
			N_{2s}	N_{2p}	O_{2s}	O_{2p}	N_{2s}	N_{2p}	O_{2s}	O_{2p}	N_{2s}	N_{2p}	O_{2s}	O_{2p}
$1a_2'$ }	5.6					.67				.75				.67
$1e''$ }						1.33				1.51				1.33
$4e'$	7.5	1.5		.55	.02	1.13		.46	.36	1.37		.37		1.21
$3e'$	11.9	1.7		1.50	.41	.42		.96	.99	.41		.76	.53	.55
$1a_2''$	13.3	3		.60		.47		1.00		.15		1.26		.25
$4a_1'$	14.5	2	.72		.37	.05	.59		.51	.11	.31		.38	.18
$2e'$	26.2	4		1.00	.93	.07		.50	.91	.12		.89	.89	.14
$3a_1'$	31.7	3	.85		.29	.09	.44		.32	.04	.31		.43	.13
Total			1.57	3.69	2.02	4.23	1.03	2.92	3.10	4.46	.62	3.28	2.23	4.46
N_{1s}	407.5	.2												
Charge N/O			-.26		-.25						+1.09		-.69	

[a]Orbitals labeled according to D_{3h} symmetry.
[b]XPS binding energies given by Kosuch et. al. (19).
[c]Widths as estimated from XPS and XES data (19,20).
[d]Electrons per atom as reported by Dolin and Dyatkina (16).
[e]Electrons per atom (local and Mulliken) as determined by our X_α calculations.

Table 3. Comparison of M.O. Populations with Experimental Data

Orbital Type		Nitrogen K_α				Oxygen K_α			
		X_α Local	X_α Mulliken	pp	Exp[b]	X_α Local	X_α Mulliken	XPS[a]	Exp[b]
N_p { $4e'$		15	11	15	8	82	72	74	71
N_p { $3e'$, $1a_2''$		67	62	58	81	13	18	20	18
N_p' $2e'$		17	27	27	11	2	4	1	3
O_{2p} { $4e'$, $1e''$, $1a_2'$						2	3	2	3
O_{2p} { $3e'$, $1a_2''$						1	3	2	4
O_{2s} { $4a_1'$									
O_{2s} { $2e'$									
O_{2s} { $3a_1'$									
$O_{2p(nb)}$ $1e''$, $1a_2'$						18	11	11	12
N_p { $4e'$						26	20	16	14
N_p $O_{2p(b)}$ { $1a_2''$						18	19	22	21
$N_{p\pi}$ { $3e'$									
N_s { $4a_1'$						37	32	32	39
N_p O_{2s} { $2e'$						11	18	18	12
N_s' { $3a_1'$									
$O_{2p(nb)}$ $1e''$, $1a_2'$						18	11	11	12
N_p { $4e'$						26	20	16	14
N_p $O_{2p(b)}$ { $1a_2''$						18	19	22	21
$N_{p\pi}$ { $3e'$									
N_s { $4a_1'$						37	32	32	39
N_p O_{2s} { $2e'$						11	18	18	12
N_s' { $3a_1'$									

[a]XPS matrix elements from Calabrese and Hayes (20) (i.e., N_{2s} = 8.8, N_{2p} = .8, O_{2s} = 10.3, O_{2p} = 1.0).
[b]N and O K_α data from Kosuch (19), XPS data from Calabrese and Hayes (20).
[c]Empirical populations as described in text.

Table 4. Empirical Populations as Determined from the XES, XPS, and AES Data

Orbital	N_s	N_p	O_s	O_p
$1a_2'$				.67
$1e''$				1.33
$4e'$		.5	.03	1.13
$3e'$		1.04	.35	.63
$1a_2''$		1.45		.18
$4a_1'$	.70		.33	.12
$2e'$		.60	1.00	.13
$3a_1'$	.90		.17	.20
Total	1.60	3.59	1.88	4.39
Charge N/O	-.19		-.27	

Table 5. Theoretical Auger Transition Parameters as Determined from the Empirical Populations

Final State		I^a	E (eV)	Γ (eV)	N atom char.		I^a
$3a_1$	$3a_1$	3.0	332	6	s	s	3.0
	$2e'$	2.6	338	15		p	2.6
	$4a_1'$	4.7	360	5		s	4.7
	$3e''$	4.6	355	6		p	
	$1a_2''$	6.4	352	9		p	13.2
	$4e'$	2.2	358	7		p	
$2e'$	$2e'$	1.9	343	10	p	p	1.9
	$4a_1'$	2.1	358	8		s	2.1
	$3e''$	6.6	361	8		p	
	$1a_2''$	6.6	359	6		p	16.4
	$4e'$	3.2	364	8		p	
$4a_1'$	$4a_1'$	1.8	371	4	s	s	1.8
	$3e''$	3.6	373	5		p	
	$1a_2''$	5.0	370	7		p	10.3
	$4e'$	1.7	378	4		p	
$3e''$	$3e''$	5.7	376	4	p	p	
	$1a_2''$	11.3	373	5		p	37.0
	$4e'$	5.5	380	5		p	
$1a_2''$	$1a_2''$	14.5	371	6	p	p	
	$4e'$	5.4	378	5		p	5.4
$4e'$	$4e'$	1.3	384	3	p	p	1.3

[a] Total intensity normalized to 100. Auger matrix elements are: ss = 1.0, sp = 1.31, p_xp_y = p_yp_y = p_zp_z = 1.85 and p_xp_y = p_xz = p_{yz} = 2.0 (3,5). The intensities do not include the shake Auger satellite contributions.

Figure Captions

Fig. 1. Comparison of experimental N KVV Auger data, N(E): EEA/LID) $NaNO_3$ single crystal stimulated by 2000 eV electrons and analyzed in the Lock-in-Derivative mode; EEA/PC) Powdered $NaNO_3$ pressed on In, stimulated by 2000 eV electrons, analyzed in the pulse count mode; XES/PC) Powdered $NaNO_3$ stimulated by X-rays from Mg anode, 1254 eV, analyzed in the PC mode.

Fig. 2. Comparison of experimental N KVV Auger lineshapes $A_t(E)$ after subtracting off the background and removing the loss contributions by deconvolution. Plots are labeled as in Fig. 1.

Fig. 3. Comparison of the experimental XES lineshape with total (Auger + shake) theoretical lineshape as determined by the local and Mulliken X_α populations.

Fig. 4. a) Comparison of the experimental XEA lineshape with the total (Auger + shake) theoretical lineshape as determined by the empirical populations.

b) The separate Auger and the shake satellite contribution compared to the experimental lineshape. The shake satellites contribute 35% of the total intensity.

c) Comparison of the theoretical shake satellite lineshape with the 'experimental' shake lineshape. The 'experimental' shake lineshape is assumed to be the difference between the total experimental and the theoretical Auger lineshapes.

d) Comparison of the N ss, N sp and N pp contributions to the Auger lineshape.

e) Comparison of the N ss, N sp and N pp contributions to the shake-Auger lineshape.

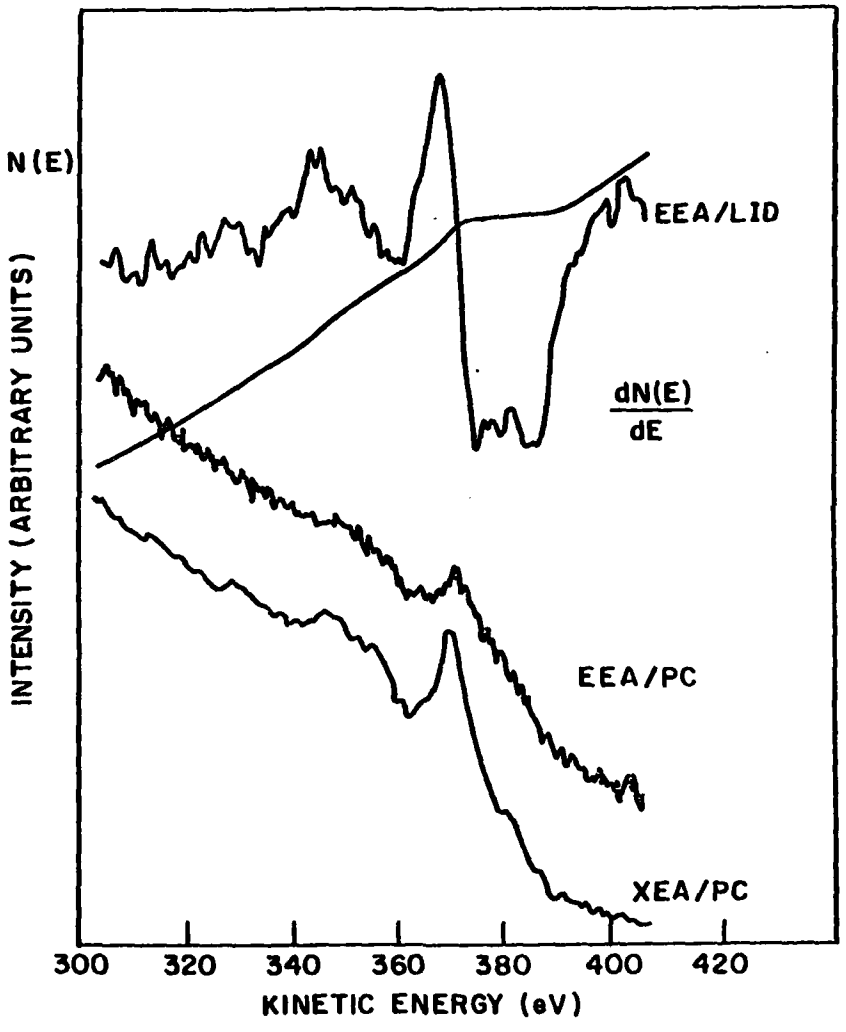

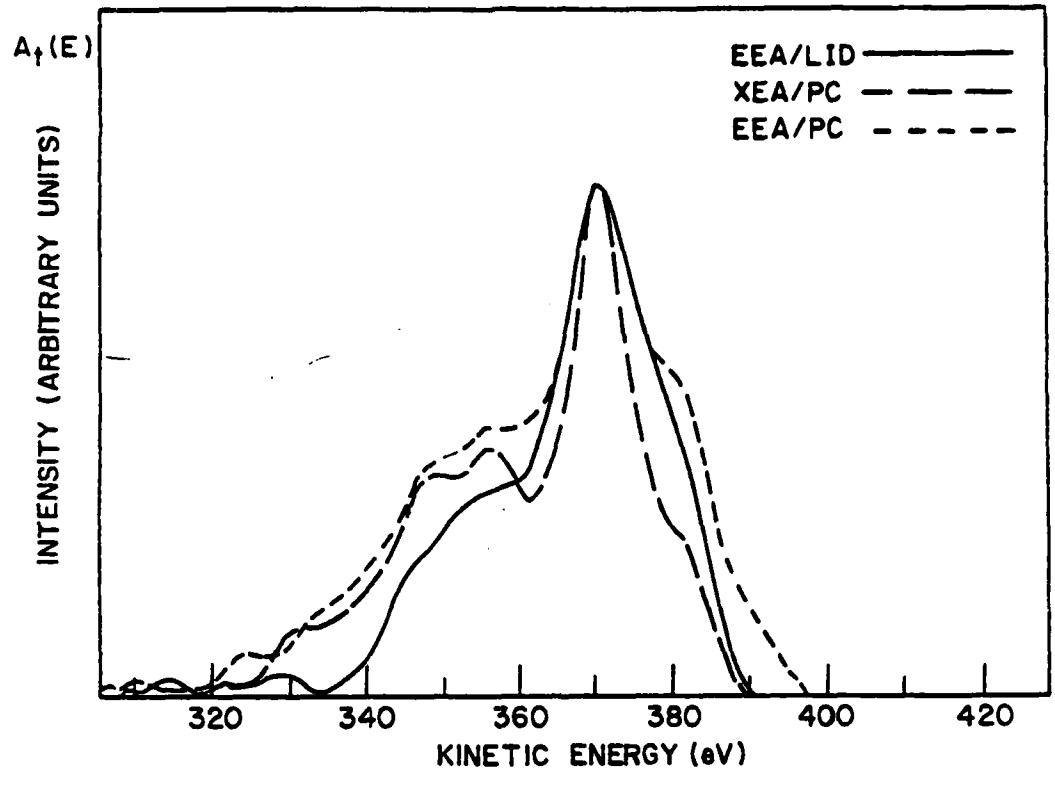
$A_t(E)$
INTENSITY (ARBITRARY UNITS)
EEA/LID
XEA/PC
EEA/PC
320
340
360
380
400
420
KINETIC ENERGY (eV)

2

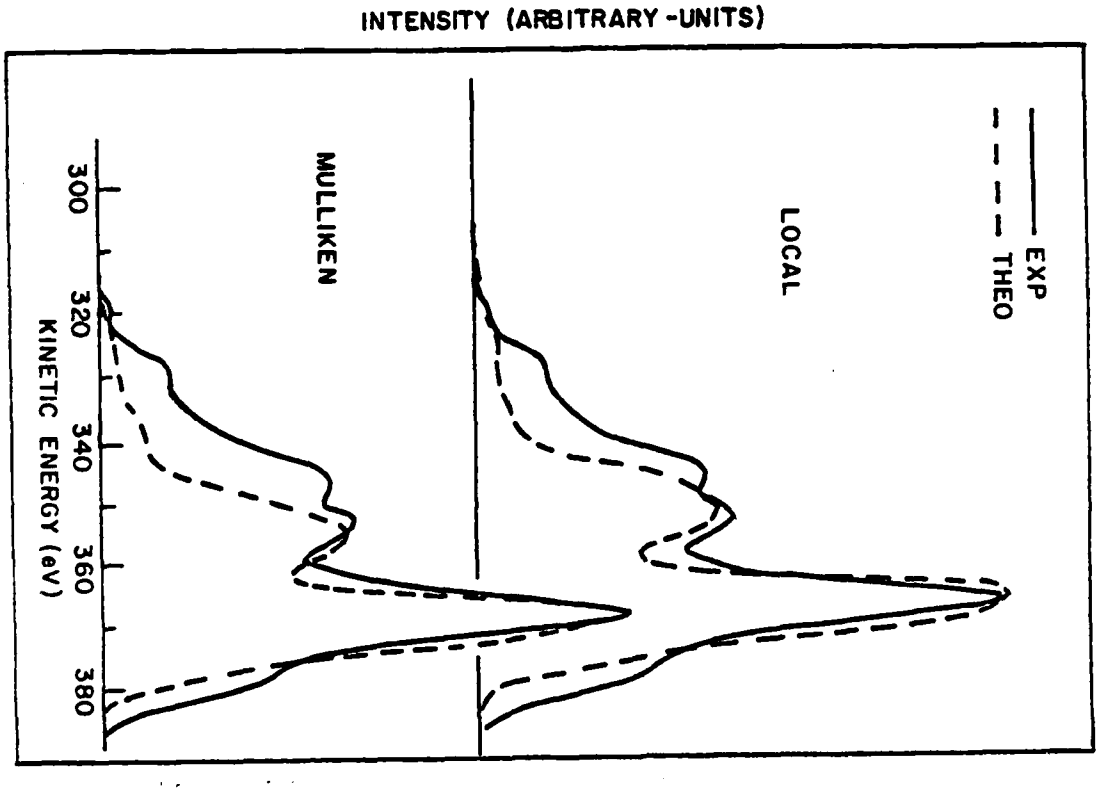
INTENSITY (ARBITRARY-UNITS)
MULLIKEN
LOCAL
EXP
THEO
300
320
340
360
380
KINETIC ENERGY (eV)

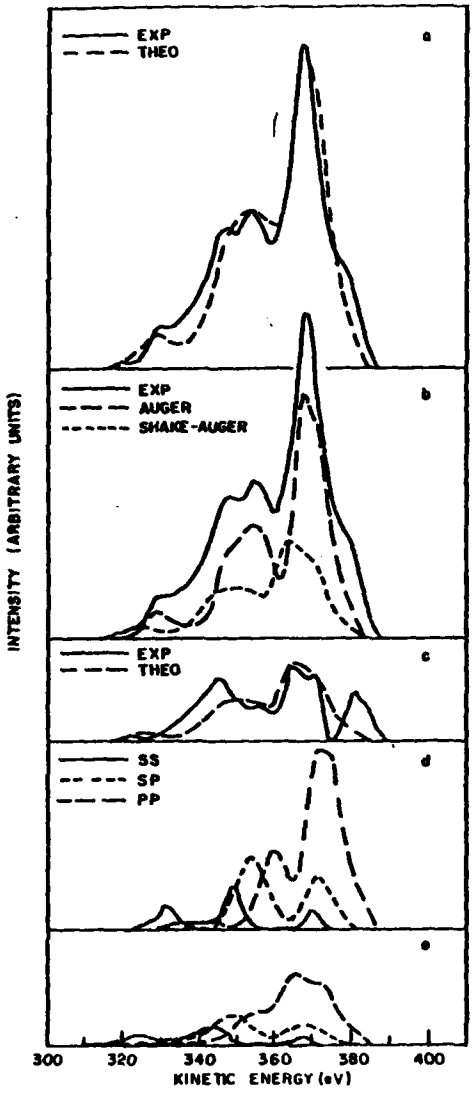
EXP
THEO
a
EXP
AUGER
SHAKE-AUGER
b
EXP
THEO
c
SS
SP
PP
d
e
INTENSITY (ARBITRARY UNITS)
300
320
340
360
380
400
KINETIC ENERGY (eV)

TECHNICAL REPORT DISTRIBUTION LIST, GEN

	No. Copies
Office of Naval Research Attn: Code 472 800 North Quincy Street Arlington, Virginia 22217	2
ONR Western Regional Office Attn: Dr. R. J. Marcus 1030 East Green Street Pasadena, California 91106	1
ONR Eastern Regional Office Attn: Dr. L. H. Peebles Building 114, Section D 666 Summer Street Boston, Massachusetts 02210	1
Director, Naval Research Laboratory Attn: Code 6100 Washington, D.C. 20390	1
The Assistant Secretary of the Navy (RE&S) Department of the Navy Room 4E736, Pentagon Washington, D.C. 20350	1
Commander, Naval Air Systems Command Attn: Code 310C (H. Rosenwasser) Department of the Navy Washington, D.C. 20360	1
Defense Technical Information Center Building 5, Cameron Station Alexandria, Virginia 22314	12
Dr. Fred Saalfeld Chemistry Division, Code 6100 Naval Research Laboratory Washington, D.C. 20375	1
U.S. Army Research Office Attn: CRD-AA-IP P.O. Box 1211 Research Triangle Park, N.C. 27709	1
Naval Ocean Systems Center Attn: Mr. Joe McCartney San Diego, California 92152	1
Naval Weapons Center Attn: Dr. A. B. Amster, Chemistry Division China Lake, California 93555	1
Naval Civil Engineering Laboratory Attn: Dr. R. W. Drisko Port Hueneme, California 93401	1
Department of Physics & Chemistry Naval Postgraduate School Monterey, California 93940	1
Scientific Advisor Commandant of the Marine Corps (Code RD-1) Washington, D.C. 20380	1
Naval Ship Research and Development Center Attn: Dr. G. Bosmajian, Applied Chemistry Division Annapolis, Maryland 21401	1
Naval Ocean Systems Center Attn: Dr. S. Yamamoto, Marine Sciences Division San Diego, California 91232	1
Mr. John Boyle Materials Branch Naval Ship Engineering Center Philadelphia, Pennsylvania 19112	1

TECHNICAL REPORT DISTRIBUTION LIST, 056

	No. Copies
Dr. G. A. Somorjai Department of Chemistry University of California Berkeley, California 94720	1
Dr. L. N. Jarvis Surface Chemistry Division 4555 Overlook Avenue, S.W. Washington, D.C. 20375	1
Dr. J. B. Hudson Materials Division Rensselaer Polytechnic Institute Troy, New York 12181	1
Dr. John T. Yates Surface Chemistry Section National Bureau of Standards Department of Commerce Washington, D.C. 20234	1
Dr. Theodore E. Madey Surface Chemistry Section Department of Commerce National Bureau of Standards Washington, D.C. 20234	1
Dr. J. M. White Department of Chemistry University of Texas Austin, Texas 78712	1
Dr. Keith H. Johnson Department of Metallurgy and Materials Science Massachusetts Institute of Technology Cambridge, Massachusetts 02139	1
Dr. J. E. Demuth IBM Corporation Thomas J. Watson Research Center P.O. Box 218 Yorktown Heights, New York 10598	1
Dr. C. P. Flynn Department of Physics University of Illinois Urbana, Illinois 61801	1
Dr. W. Kohn Department of Physics University of California (San Diego) LaJolla, California 92037	1
Dr. R. L. Park Director, Center of Materials Research University of Maryland College Park, Maryland 20742	1
Dr. W. T. Peria Electrical Engineering Department University of Minnesota Minneapolis, Minnesota 55455	1
Dr. Chia-wei Woo Department of Physics Northwestern University Evanston, Illinois 60201	1
Dr. D. C. Mattis Polytechnic Institute of New York 333 Jay Street Brooklyn, New York 11201	1
Dr. Robert M. Hexter Department of Chemistry University of Minnesota Minneapolis, Minnesota 55455	1
Dr. R. P. Van Duyne Chemistry Department Northwestern University Evanston, Illinois 60201	1

	No. Copies
Dr. S. Sibener Department of Chemistry James Franck Institute 5640 Ellis Avenue Chicago, Illinois 60637	1
Dr. M. G. Lagally Department of Metallurgical and Mining Engineering University of Wisconsin Madison, Wisconsin 53706	1
Dr. Robert Gomer Department of Chemistry James Franck Institute 5640 Ellis Avenue Chicago, Illinois 60637	1
Dr. R. G. Wallis Department of Physics University of California, Irvine Irvine, California 92664	1
Dr. D. Ramaker Chemistry Department George Washington University Washington, D.C. 20052	1
Dr. P. Hansma Chemistry Department University of California, Santa Barbara Santa Barbara, California 93106	1
Dr. P. Hendra Chemistry Department Southampton University England SO9JNH	1
Professor P. Skell Chemistry Department Pennsylvania State University University Park, Pennsylvania 16802	1
Dr. J. C. Hemminger Chemistry Department University of California, Irvine Irvine, California 92717	1
Dr. Martin Fleischmann Department of Chemistry Southampton University Southampton SO9 5NH Hampshire, England	1
Dr. J. Osteryoung Chemistry Department State University of New York at Buffalo Buffalo, New York 14214	1
Dr. G. Rubloff I.B.M. Thomas J. Watson Research Center P. O. Box 218 Yorktown Heights, New York 10598	1
Dr. J. A. Gardner Department of Physics Oregon State University Corvallis, Oregon 97331	1
Dr. G. D. Stein Mechanical Engineering Department Northwestern University Evanston, Illinois 60201	1
Dr. K. G. Spears Chemistry Department Northwestern University Evanston, Illinois 60201	1
Dr. R. W. Plummer University of Pennsylvania Department of Physics Philadelphia, Pennsylvania 19104	1
Dr. E. Yeager Department of Chemistry Case Western Reserve University Cleveland, Ohio 41106	2
Professor D. Hercules University of Pittsburgh Chemistry Department Pittsburgh, Pennsylvania 15260	1

	No. Copies
Professor N. Winograd The Pennsylvania State University Department of Chemistry University Park, Pennsylvania 16802	1
Professor T. F. George The University of Rochester Chemistry Department Rochester, New York 14627	1
Professor Dudley R. Herschbach Harvard College Office for Research Contracts 1350 Massachusetts Avenue Cambridge, Massachusetts 02138	1
Professor Horia Metiu University of California, Santa Barbara Chemistry Department Santa Barbara, California 93106	1
Professor A. Steckl Rensselaer Polytechnic Institute Department of Electrical and Systems Engineering Integrated Circuits Laboratories Troy, New York 12181	1
Professor R. D. Archer University of Massachusetts Chemistry Department Amherst, Massachusetts 01003	1
Dr. A. C. Pastor Hughes Research Laboratories 3011 Malibu Canyon Road Malibu, California 90265	1